# Indicative Mapping of Rice Cropping Systems in Timor-Leste Using PlanetScope NDVI Time Series and DTW Clustering

Pedro J.F. [1*], Masahiko N.[1,2]

[1]Graduate School of Science and Technology for Innovation, Yamaguchi University, 2-16-1, Ube 755-8611, Yamaguchi, Japan

[2]Center for Research and Application of Satellite Remote Sensing, Yamaguchi University, 2-16-1, Tokiwadai, Ube 755-8611, Yamaguchi, Japan.

d002wdu@yamaguchi-u.ac.jp

***Abstract:*** *Monitoring rice cropping systems and their seasonal dynamics is crucial for assessing production and planning, particularly in regions with limited field observations. We introduce a hexagonal grid-based time-series framework that segments rice-growing patterns and phenology in Timor-Leste using monthly 3 m PlanetScope imagery. The Normalized Difference Vegetation Index (NDVI) was extracted for approximately 6,000 hexagonal grid cells (50 m) from December 2018 to September 2022 and clustered using Dynamic Time Warping (DTW) to group similar growth trajectories. The optimal number of phenological regimes was determined by a majority decision across internal validity indices: Silhouette, Davies–Bouldin, and Calinski–Harabasz. These indices consistently favored two clusters, although the Elbow curve indicated a bend near three. For agronomic interpretation, we summarized each cluster's NDVI profile into phenology metrics, including mean, max, min, amplitude, counts of low-cover months below 0.45, sustained greenness above 0.55, and peaks at or above 0.60, and assigned functional labels. The analysis identified two temporally stable regimes aligned with the national cropping calendar: (1) a single-crop system with one main-season green-up from December to May and predominantly low off-season NDVI below 0.45, and (2) an irrigated double-crop system maintaining elevated off-season greenness, with NDVI frequently at or above 0.60 for multiple months from June to November, indicating a second cycle. The results indicate that DTW clustering of satellite NDVI can effectively delineate dominant phenology and distinguish between single and double rice cropping in data-scarce settings. While the workflow is scalable and transferable, findings are indicative rather than definitive due to limited ground truth. Future work should incorporate plot-level observations, such as sowing and harvest dates, irrigation records, and GPS photo points, to calibrate labels and quantify accuracy. This study presents a practical approach to operational phenology mapping, which can inform irrigation management and seasonal monitoring in similar environments.*

*Keywords: ndvi#1, dtw clustering#2, time series analysis#3, rice crop system#4, Timor-Leste#5*

**Introduction**

Rice (Oryza sativa L.) is a primary staple for much of the world, with production and consumption concentrated in Asia (Hossain, 2000; Fairhurst et al., 2002; Sasaki, 2019). In Timor-Leste, domestic harvest has not consistently met national needs, leaving the country dependent on imports and exposed to price and climate variability that complicate food-security planning (Food and Agriculture Organization of the United Nations, n.d.; Fox, 2003; World Bank, 2023). These structural pressures are compounded by patchy statistics and limited field observations, underscoring the need for stronger agricultural information systems to support timely, evidence-based decisions (Food and Agriculture Organization of the United Nations, 2019).

Satellite Earth-observation time series offer a practical way to narrow these information gaps by repeatedly tracking vegetation dynamics across space and administrative boundaries 9 Zhang et al., 2003; Zhang, Friedl, & Schaaf, 2006). The Normalized Difference Vegetation Index (NDVI), derived from red and near-infrared reflectance, provides a physically interpretable signal of canopy condition and has long been used to describe crop phenology under variable weather and cloud conditions (Bhatti et al., 2024; Essaadia et al., 2022; Reed et al., 1994). For spatial aggregation and analysis, hexagonal grids are advantageous because each cell has equal-distance neighbors, which reduces edge effects and yields more coherent neighborhood definitions in ecological and land-surface studies (Birch et al., 2007).

When planting dates and crop cycles vary across regions, direct comparison of seasonal trajectories can be misleading unless timing differences are addressed. Dynamic Time Warping (DTW) aligns sequences along the time axis and, when paired with NDVI trajectories, has been effective for mapping rice systems that follow flexible calendars, including applications at national scale (Guan et al., 2016). Because unsupervised clustering is sensitive to the number and composition of groups, internal validation is essential to assess separation and compactness; widely used diagnostics include the Silhouette, Davies–Bouldin, and Calinski–Harabasz indices [17–19]. In monsoon-affected agroecosystems, vegetation greenness typically follows the availability of water, and irrigated and rain-fed rice fields often show distinct seasonal persistence and timing of green-up and senescence [20–22].

In this study, we integrate high-resolution PlanetScope NDVI time series with DTW-based K-Means on a boundary-free hexagonal grid to characterize rice phenology and cropping systems in Timor-Leste. We evaluate the resulting phenological regimes with established internal indices and translate cluster profiles into agronomically interpretable classes using simple, transparent NDVI-based rules. The spatial patterns align with the country's established main-

season and off-season windows and distinguish areas consistent with single-cropping from those exhibiting characteristics of irrigated double-cropping. The contribution is a label-light, scalable workflow for operational phenology mapping that can inform irrigation scheduling, input allocation, and climate-risk management in data-scarce settings (Shang et al., 2017).

**Literature Review**

The Normalized Difference Vegetation Index (NDVI), derived from red and near-infrared reflectance, is a robust and physically interpretable indicator of vegetation vigor. NDVI effectively captures canopy density and photosynthetic activity across both spatial and temporal scales. Its sensor-independent formulation and strong empirical association with crop growth dynamics have established NDVI as a standard metric for monitoring agricultural systems, including rice, at multiple scales. The increasing availability of high-revisit, high-resolution satellite constellations enhance the utility of NDVI by enabling the detection of field-scale heterogeneity and management practices that are often undetectable in coarser-resolution products.

Hexagonal grids provide advantages over square grids for spatial aggregation because each cell has six equidistant neighbors. This configuration reduces directional bias and edge effects, resulting in more isotropic neighborhood definitions for ecological and land-surface analyses (Birch et al., 2007). Such properties are particularly beneficial when aggregating dense, high-resolution time series into consistent analysis units that preserve local spatial structure and remain independent of administrative boundaries.

Dynamic Time Warping (DTW) provides an elastic measure of similarity between temporal sequences by permitting non-linear alignments along the time axis. When applied to NDVI trajectories, DTW enables clustering of fields or grid cells that exhibit similar phenological patterns, even when events occur at different times across locations or years. Previous studies have demonstrated that DTW applied to NDVI time series is effective for delineating rice cropping systems with flexible and heterogeneous schedules, including national-scale applications such as in Vietnam, where asynchronous planting and management complicate conventional comparisons (Guan et al., 2016). In this context, combining DTW with partitioning algorithms, such as K-Means, on DTW distances supports the identification of coherent phenological regimes without requiring supervision or extensive reliance on ancillary labels.

Robust evaluation of unsupervised cluster structures typically employs complementary internal validity indices. The Silhouette index measures the relative cohesion and separation of clusters. The Davies–Bouldin index penalizes overlapping or poorly separated clusters, while the Calinski–Harabasz index favors compact, well-separated partitions [17–19]. Considering these diagnostics together supports parsimonious and interpretable solutions by balancing model simplicity with empirical separation, which is essential for operational mapping in data-scarce environments.

The literature identifies three primary best practices for clustering agricultural time-series data: using NDVI or similar indices to monitor plant growth, selecting spatial units such as hexagonal grids to minimize edge effects and preserve local patterns, and employing DTW-based clustering to accommodate variations in crop timing. Careful internal validation is then applied to determine the optimal number of clusters. Collectively, these steps facilitate the identification of stable and meaningful crop patterns, such as distinguishing between single- and double-cropping rice systems, without reliance on fixed calendars or extensive field data.

Building on these approaches, this study applies high-resolution NDVI data and a DTW-based K-Means method on a hexagonal grid to map rice growth and cropping systems in Timor-Leste. Cluster quality is assessed using the Silhouette, Davies–Bouldin, and Calinski–Harabasz indices to identify a clear and meaningful solution that aligns with field expectations. This method aims to provide transparent and repeatable mapping in data-limited contexts, supporting previous findings that clustering by growth patterns can identify cropping systems in regions with limited data.

## Methodology

### a. Brief Introduction to the Study Area

Maliana lies in Bobonaro's low-lying rice plain, an alluvial clay basin (<100 m a.s.l.) fed by the Bulobu, Nunura, and Malibaka rivers—conditions that favor irrigated paddy and consistent canopy development detectable by satellites. Its proximity to the Indonesian border and to domestic markets supports the movement of grain and potential cross-border trade Autoridade Munisípiu Bobonaro, n.d.). Production records identify Maliana as a leading rice zone in Timor-Leste, with a planted area and yields that outpace national levels, and recent ledgers report the municipality's largest unmilled output (Correia & Sarmento, 2020; Sasaki, 2019); the FAO likewise flags the district as high-potential for paddy (Food and Agriculture Organization of the United Nations, 2021). Performance is underpinned by the Maliana-I and

Maliana-II gravity schemes, which provide perennial water to a large command area despite past flood damage. Upgrades have expanded the irrigable reach and enabled cropping intensities above one crop per year (Food and Agriculture Organization of the United Nations, 2011; National Directorate for Agriculture and Horticulture et al., 2015). Together, the basin's hydrology, infrastructure, and market access make Maliana a representative, operational setting for NDVI time-series analysis and DTW-based phenology clustering.

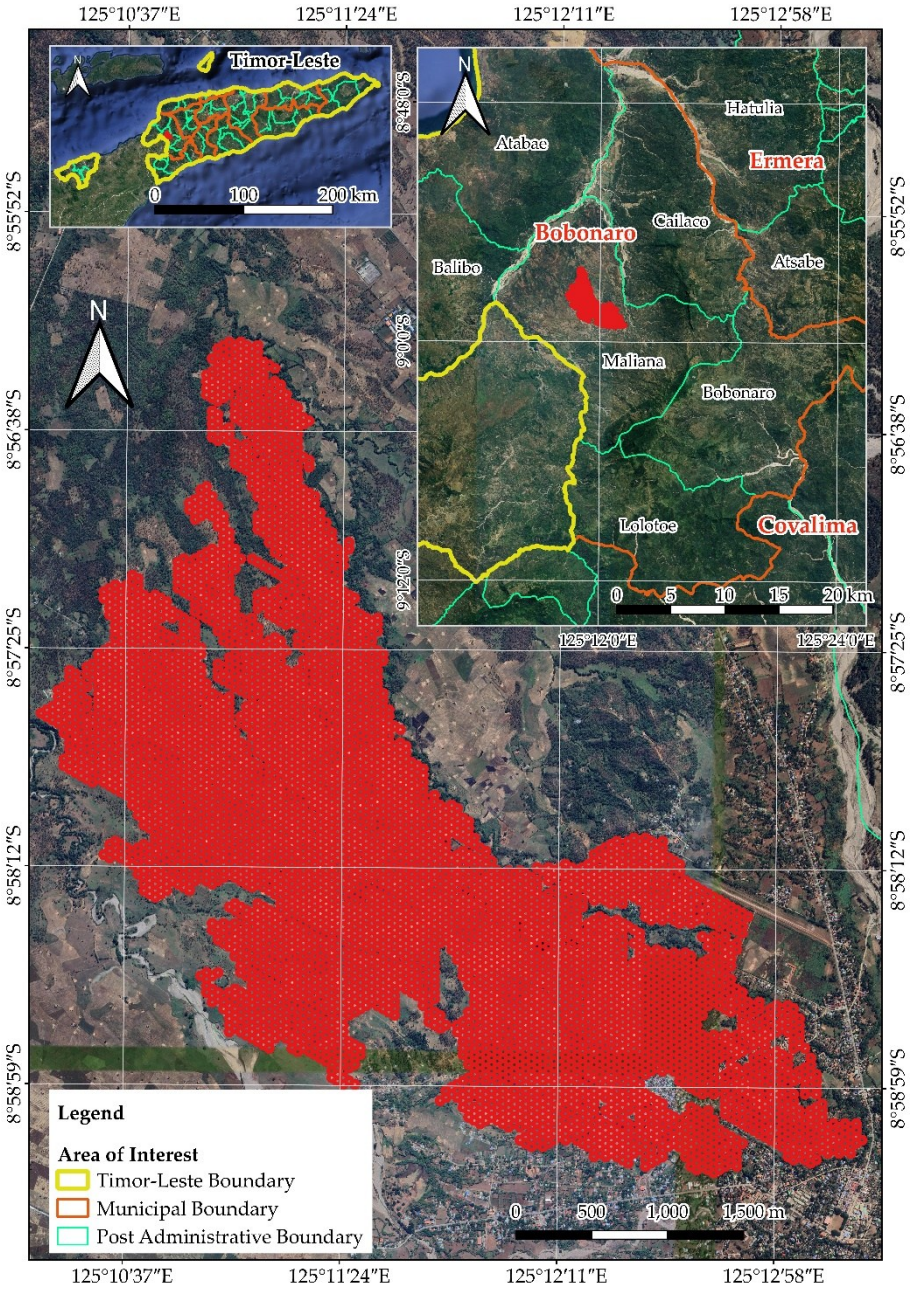


Figure1: Study area in Bobonaro Municipality, Timor-Leste, showing the area of interest within national, municipal, and post-administrative boundaries.

**b. PlanetScope NDVI Time Series Imagery**

PlanetScope multispectral scenes (PSScene-Surface Reflectance) from Planet Labs Inc. were acquired for each clear-sky day between December 2018 and September 2022. Each CubeSat in the constellation captures four spectral bands: blue, green, red, and near-infrared (NIR), at approximately 3-meter pixel size. This spatial resolution allows for the identification of individual paddy blocks and smallholder fields.

All scenes are orthorectified and atmospherically corrected to surface reflectance. Each scene is accompanied by quality metadata, including acquisition time, sun and sensor geometry, and cloud cover. Metadata were reviewed to exclude images with more than 20 percent cloud coverage or severe off-nadir views.

For every retained scene, we computed the Normalized Difference Vegetation Index (NDVI) using,

$$NDVI = \frac{\rho NIR - \rho Red}{\rho NIR + \rho Red} \quad (1)$$

where $\rho NIR$ and $\rho Red$ represent surface reflectance values from the near-infrared and red spectral bands, respectively.

The variables in the NDVI formula represent surface reflectance values from the near-infrared and red spectral regions. NDVI derived from high-resolution PlanetScope imagery offers significant advantages for monitoring rice crop development, health, and stress responses. The near-daily revisit frequency and meter-level spatial resolution of PlanetScope imagery support the detection of subtle and short-term changes in rice crop phenology. These phenological changes encompass critical stages, including transplanting, panicle initiation, and senescence (Houborg & McCabe, 2016). NDVI is strongly correlated with canopy chlorophyll content and structural variation, making it a reliable indicator of rice crop vigor and physiological stress (Xue & Su, 2017). In rice production systems, NDVI time series capture dynamic phenological phases and environmental stresses such as flooding and drought Xiao et al., 2010).

Combining NDVI with other vegetation indices enables the discrimination of rice diseases at the sub-field scale, thereby enhancing its application in precision agriculture (Shi et al., 2018). The NDVI raster generated from PlanetScope imagery serves as a primary input for the time-series phenological analysis and clustering workflows in this study.

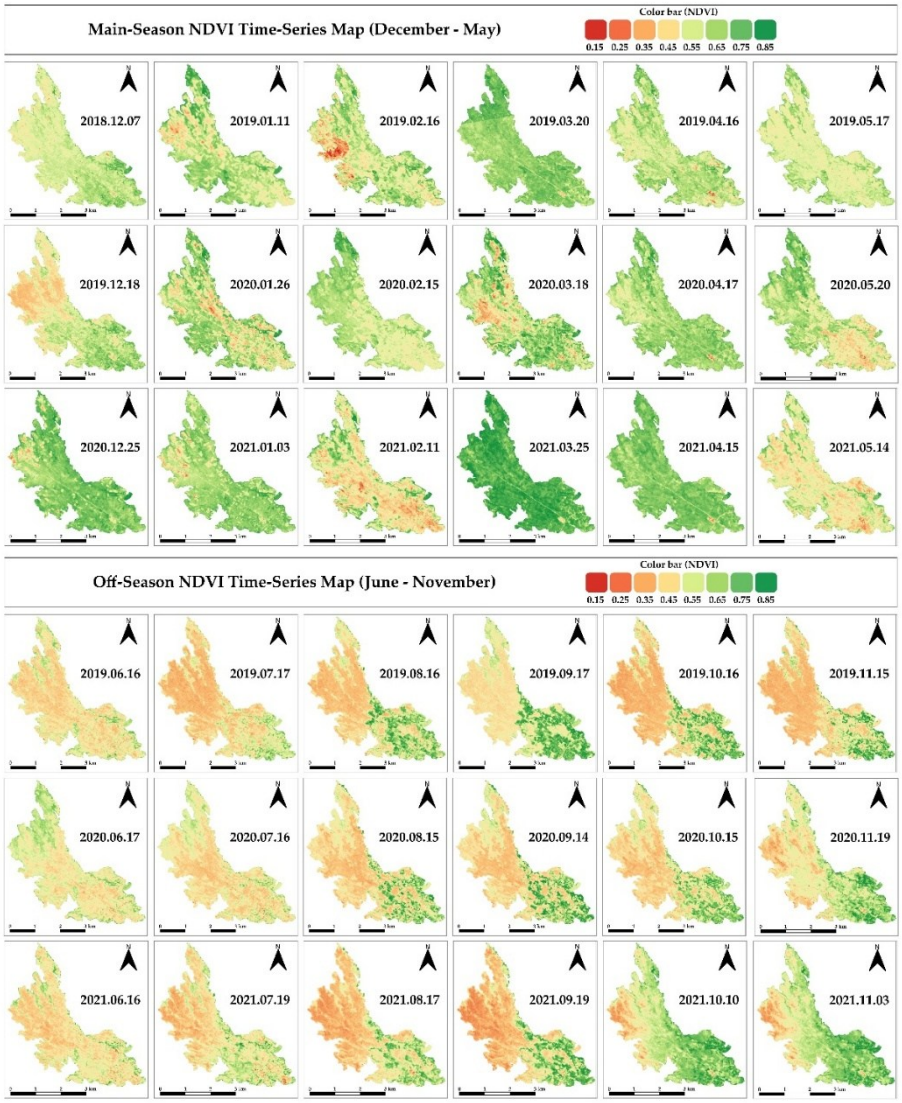


Figure 2: Seasonal PlanetScope NDVI (3 m) time-series maps for Maliana, Timor-Leste: (top) main-season snapshots and (bottom) off-season snapshots. The color bar indicates NDVI (0.15–0.85).

### c. Hexagon-Based Sampling and NDVI Time-Series Extraction

A unified QGIS workflow was implemented to integrate hexagonal grid generation with scene-wise zonal statistics, resulting in an analysis-ready NDVI time series for each field unit. The process began with the creation of a continuous hexagonal grid using Vector, Research Tools, and the Create Grid function in WGS 84 / UTM Zone 51S (EPSG: 32751). Each hexagon had a 25-meter edge length and was assigned a unique identifier ranging from 1 to 6,000. The grid was intersected with the current land-cover layer, and hexagons overlapping forest, urban, or open water areas were excluded to ensure that only cultivated parcels were included in the summary. The use of hexagonal geometry reduces edge effects and provides more uniform

neighborhood relationships compared to square grids, thereby enhancing spatial consistency for subsequent clustering.

For each cloud-free PlanetScope NDVI scene, raster and zonal statistics were executed in batch mode to calculate the mean NDVI for every retained hexagon on the corresponding acquisition date. Each scene produced a CSV file with two columns: hexagon ID and mean NDVI for that date. All scene-specific tables were merged by hexagon ID into a comprehensive matrix, with rows representing hexagons and columns representing acquisition dates over the 46-month period. This workflow produces a high-resolution NDVI data cube that consistently captures rice-field dynamics in both spatial and temporal dimensions, minimizes contamination from non-agricultural pixels, and is suitable for DTW-based clustering, phenology metric extraction, and cropping-system classification.

### d. Time-Series Clustering Using DTW-Based K-Means

We clustered monthly NDVI series per hexagon using k-means++ with Dynamic Time Warping (DTW) as the distance metric, which groups pixels by phenological shape while tolerating temporal shifts—consistently outperforming Euclidean distance in remote-sensing time series (GeeksforGeeks, n.d.; Lampert et al., 2019; Mure et al., 2016; Zhang & Hepner, 2017). NDVI for each cell was min–max scaled to [0, 1] to emphasize temporal patterns over absolute levels, then input into DTW-k-means to derive centroid phenologies (DTW barycenters) and assign cluster labels. The number of clusters was determined through internal validation (Elbow, Silhouette, Davies–Bouldin, and Calinski–Harabasz) and centroid interpretability, resulting in compact, temporally coherent phenoregions suitable for downstream phenology metrics and cropping-system mapping.

### e. Determine the optimal value of k in K-Means Clustering

- ✓ Elbow method

The Elbow Method begins by running K-Means over a range of candidate cluster counts and plotting the within-cluster sum of squares (WCSS) (Shi et al., 2021),

$$\boldsymbol{WCSS} = \sum_{i=1}^{k} \sum_{j=1}^{n_i} \boldsymbol{distance}\,(x_j^{(i)}, c_i)^2 \qquad (2)$$

where, $(x_j^{(i)}, c_i)^2$ represents the distance between the j-th data point $x_j^{(i)}$ in cluster $i$ and the centroid $c_i$ of that cluster (Shi et al., 2021). Because the elbow can be ambiguous, we applied quantitative bend-detection heuristics to aid identification (Umaragono et al., 2019; Tajunisha & Saravanan, 2011). Practically, we computed DTW inertia (WCSS under Dynamic Time

Warping) for DTW-K-Means with k=2−8, used the elbow to narrow the plausible range, and finalized k with additional indices and agronomic interpretability.

✓ Silhouette score and Principal Component Analysis (PCA)

We applied PCA to the scaled NDVI time series to reduce dimensionality, suppress noise/collinearity, and improve cluster separability (Marín Celestino et al., 2018; Awong & Zielinska, 2023). K-means was run in the PCA space, and partitions were assessed with silhouette analysis. For each observation i, let a (i) be the mean intra-cluster dissimilarity and b (i) the minimum mean inter-cluster dissimilarity; the silhouette coefficient is:

$$s(i) = ( b(i) - a(i) ) / max\{ a(i), b(i) \} \quad (3)$$

Values near +1 indicate well-clustered points, ≈ 0 indicate boundary cases, and negative values suggest misclassification (Awong & Zielinska, 2023). We computed average silhouette widths for k = 2–5 and inspected silhouette plots alongside PCA scatter plots to judge compactness and separation.

✓ Cluster Validity Indices

We cross-validated k using the Davies–Bouldin Index (DBI) and Calinski–Harabasz Index (CHI), two standard internal metrics. DBI measures the average similarity of each cluster to its most similar neighbor as a ratio of within-cluster scatter to between-centroid separation (Davies & Bouldin, 1979),

$$DBI = (1/N) \Sigma\_\{i = 1\}\^\{N\} max\_\{i \neq j\} ( (s\_i + s\_j) / d\_\{ij\} ) \quad (4)$$

where $N$ is the number of clusters, $s_i$ is the average distance of all samples in cluster $i$ from its centroid, and $d_{ij}$ is the Euclidean distance between the centroids of cluster $i$ and $j$. Lower DBI indicate more compact and well-separated clusters (Wang & Xu, 2019). CHI evaluates the ratio of between- to within-cluster dispersion, favoring partitions with well-separated and compact clusters (Derrick & Thomas, 2004; Runge et al., 2014):

$$CH(K) = ( B(K) \cdot (N - K) ) / ( W(K) \cdot (K - 1) ) \quad (5)$$

where B(K) and W(K) are between- and within-cluster dispersions, N is the number of samples, and K the number of clusters; higher CHI is better. The final k was chosen by consensus across Elbow, average silhouette, DBI, and CHI, then DTW-KMeans was refit at that k on the full scaled dataset to assign each hexagon a phenology label for mapping and analysis.

## Results

### f. Optimal Number of Clusters

Across multiple internal criteria, k = 2 emerges as the most parsimonious and well-supported solution. While the Elbow plot indicates a bend around k ≈ 3, the majority decision across independent indices (higher average silhouette, lower Davies–Bouldin index, and higher Calinski–Harabasz index) supports selecting k = 2. In short, we adopt k = 2 by majority vote across metrics, even though the Elbow plot alone suggests k ≈ 3.

The Elbow method (Figure 3) visually suggests diminishing returns beyond k ≈ 3; however, the elbow heuristic can over-partition time-series data and should not be used in isolation. Accordingly, we prioritized a majority-vote across independent indices when determining the final k. (Kodinariya & Makwana, 2013; Thorndike, 1953).

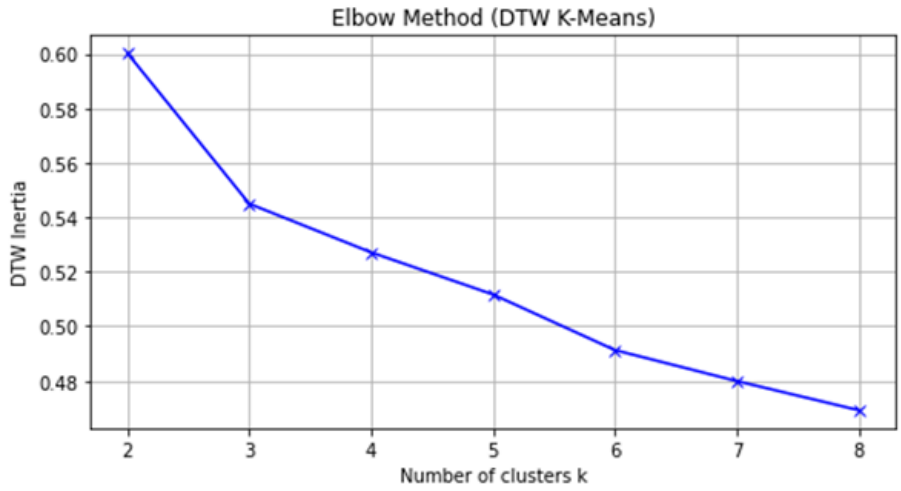


Figure 3: Elbow Method using DTW K-Means for determining the optimal number of clusters.

Silhouette analysis (Figure 4) peaks at k = 2 (0.61) and declines thereafter (0.48 at k = 3; 0.47 at k = 4; 0.42 at k = 5). Because higher silhouettes indicate better separation and compactness, this criterion favors k = 2. Given this and the corroborating internal indices, we adopt k = 2 as the final solution, while acknowledging that the Elbow plot alone points to k ≈ 3. (Rousseeuw, 1987).

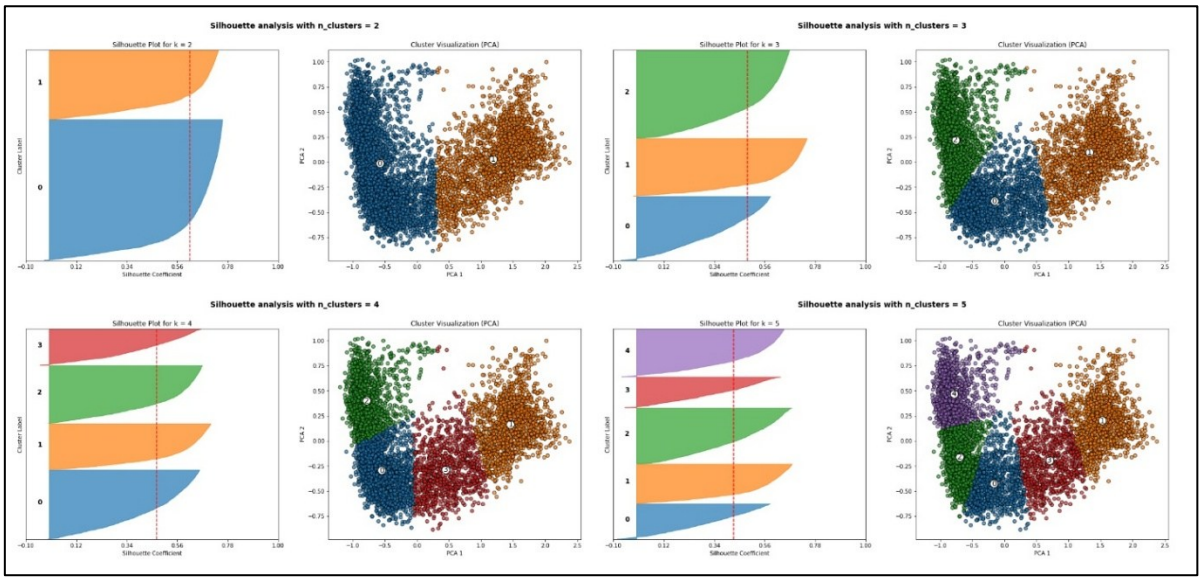


Figure 4: Silhouette analysis and PCA visualizations for k = 2, 3, 4, and 5 clusters, illustrating

Table 1: Silhouettes score for k= 2 to k=5.

| k | Silhouette |
|---|---|
| 2 | 0.61 |
| 3 | 0.48 |
| 4 | 0.47 |
| 5 | 0.42 |

Moreover, the choice of two clusters is strongly validated by internal Cluster Validity Indices (CVI). The DBI increased significantly from 1.269 at k = 2 to 2.001 at k = 3, highlighting an acceptable trade-off between compactness and separation. The worsening metrics at higher cluster counts —2.340 for k = 4 and 3.097 for k = 5 —further substantiate the decision. Similarly, the CHI drops from 3334.017 at k = 2 to 2133.629 at k = 3, with sharper declines for higher cluster numbers (1535.884 at k = 4 and 1210.814 at k = 5).

Table 2: Cluster Validity Indices for k= 2 to k=5.

| k | Davies-Bouldin | Calinski-Harabasz |
|---|---|---|
| 2 | 1.269 | 3334.017 |
| 3 | 2.001 | 2133.629 |
| 4 | 2.340 | 1535.884 |
| 5 | 3.097 | 1210.814 |

The statistical validations enabled us to map the spatial distribution of the two clusters, as shown in Figure 5, which reveals clear geographic patterns across the study area. Cluster 1 is

primarily located in the northwest, Cluster 2 encompasses the central and eastern regions, and Cluster 3 is found in the transitional zones. Figure 5 presents the temporal NDVI and rainfall profiles, highlighting how each cluster responds differently to seasonal rainfall. These spatial and temporal views make the clustering results easier to interpret and more useful.

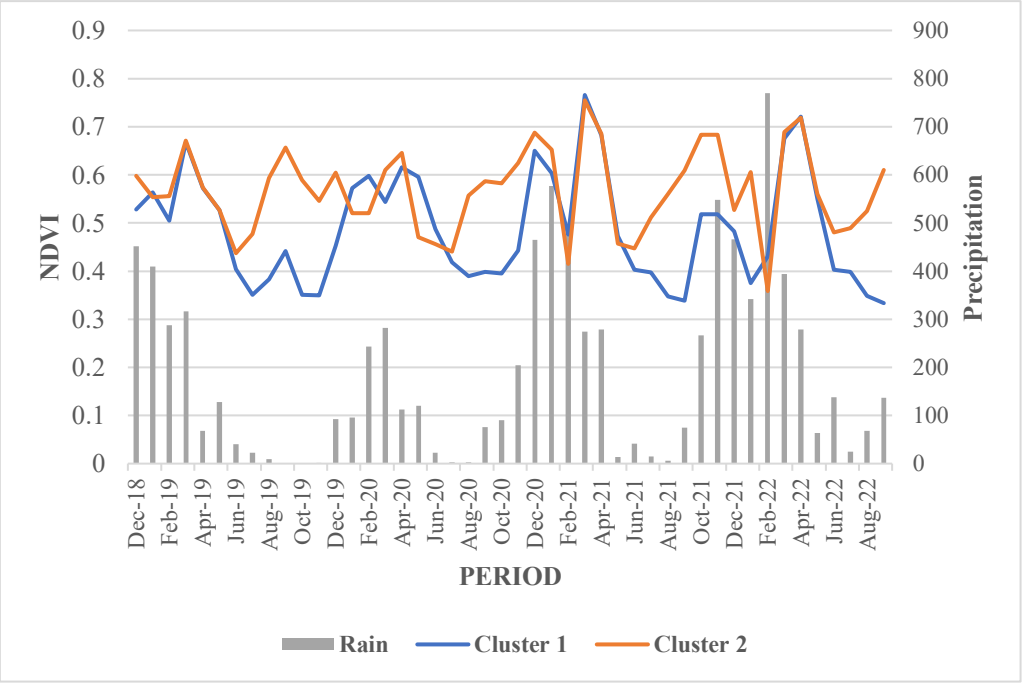


Figure 5: NDVI time-series of three clusters overlaid with precipitation data, showing the relationship between vegetation dynamics and rainfall patterns from 2018 to 2022.

**g. Crop phenology metrics and cropping systems assignment**

To convert the DTW clusters into agronomically meaningful classes, we summarized each cluster's monthly NDVI into phenology metrics—long-term mean, seasonal maximum, minimum, amplitude (max–min), counts of months with NDVI < 0.45 (fallow/low cover) and NDVI > 0.55 (sustained active canopy), the number of peaks > 0.60, and cycles $yr^{-1}$ computed from peak counts over the 46-month record (~3.83 yr). According to NASA Earth Observatory (2000), NDVI values near 0 indicate water or bare soil, ~0.2–0.3 reflect sparse vegetation, and ≥0.55–0.60 signal a closed, photosynthetically active canopy; thus, these thresholds provide a practical bridge from time-series signal to field conditions. Applied to Table 3, Cluster 1 (Avg NDVI ≈ 0.49; amplitude ≈ 0.43; 21 low-NDVI months; 8 high-NDVI months; 5 peaks → 1.30 cycles $yr^{-1}$) shows one robust green-up and peak most years followed by a prolonged low-cover period, consistent with single-cropping concentrated in the wet/main season. Cluster 2 (Avg NDVI ≈ 0.57; amplitude ≈ 0.40; 5 low-NDVI months; 17 high-NDVI months; 8 peaks → 2.09

cycles $yr^{-1}$) maintains high cover for much of the year with two distinct peaks, indicating double-cropping supported by reliable water control. Based on the Timor-Leste agricultural calendar, the within-year timing aligns with a main season in December–May and a secondary window in June–November where irrigation permits (Seeds of Life, 2010).

The spatial distribution of these assignments is shown in Figure 6, where Cluster 1 is labeled single-cropping and Cluster 2 double-cropping, providing a coherent map of cropping systems across the area of interest.

Table 3: Crop phenology metrics

| Metrics | Cluster1 | Cluster2 |
|---|---|---|
| Average NDVI | 0.4878573 | 0.56751 |
| max | 0.7658216 | 0.75486 |
| min | 0.3334182 | 0.35855 |
| Amplitude (max - min) | 0.4324033 | 0.39631 |
| Number of months < 0.45 (Dec18 - Nov19) | 6 | 1 |
| Number of months < 0.45 (Dec19 - Nov20) | 5 | 1 |
| Number of months < 0.45 (Dec20 - Nov21) | 4 | 2 |
| Number of months < 0.45 (Dec21 - Sep22) | 6 | 1 |
| Number of months > 0.55 (Dec18 - Nov19) | 3 | 8 |
| Number of months > 0.55 (Dec19 - Nov20) | 4 | 7 |
| Number of months > 0.55 (Dec20 - Nov21) | 4 | 8 |
| Number of months > 0.55 (Dec21 - Sep22) | 2 | 5 |
| Peaks > 0.6 NDVI (Dec18 - Nov19) | 1 | 2 |
| Peaks > 0.6 NDVI (Dec19 - Nov20) | 1 | 2 |
| Peaks > 0.6 NDVI (Dec20 - Nov21) | 2 | 2 |
| Peaks > 0.6 NDVI (Dec21 - Sep22) | 1 | 2 |
| % Of months < 0.45 (Dec18 – Sep22) | 21 | 5 |
| % Of months > 0.55 (Dec18 – Sep22) | 8 | 17 |
| Peaks > 0.6 NDVI (Dec18 – Sep22) | 5 | 8 |
| Cycles / year | 1.3043478 | 2.08696 |

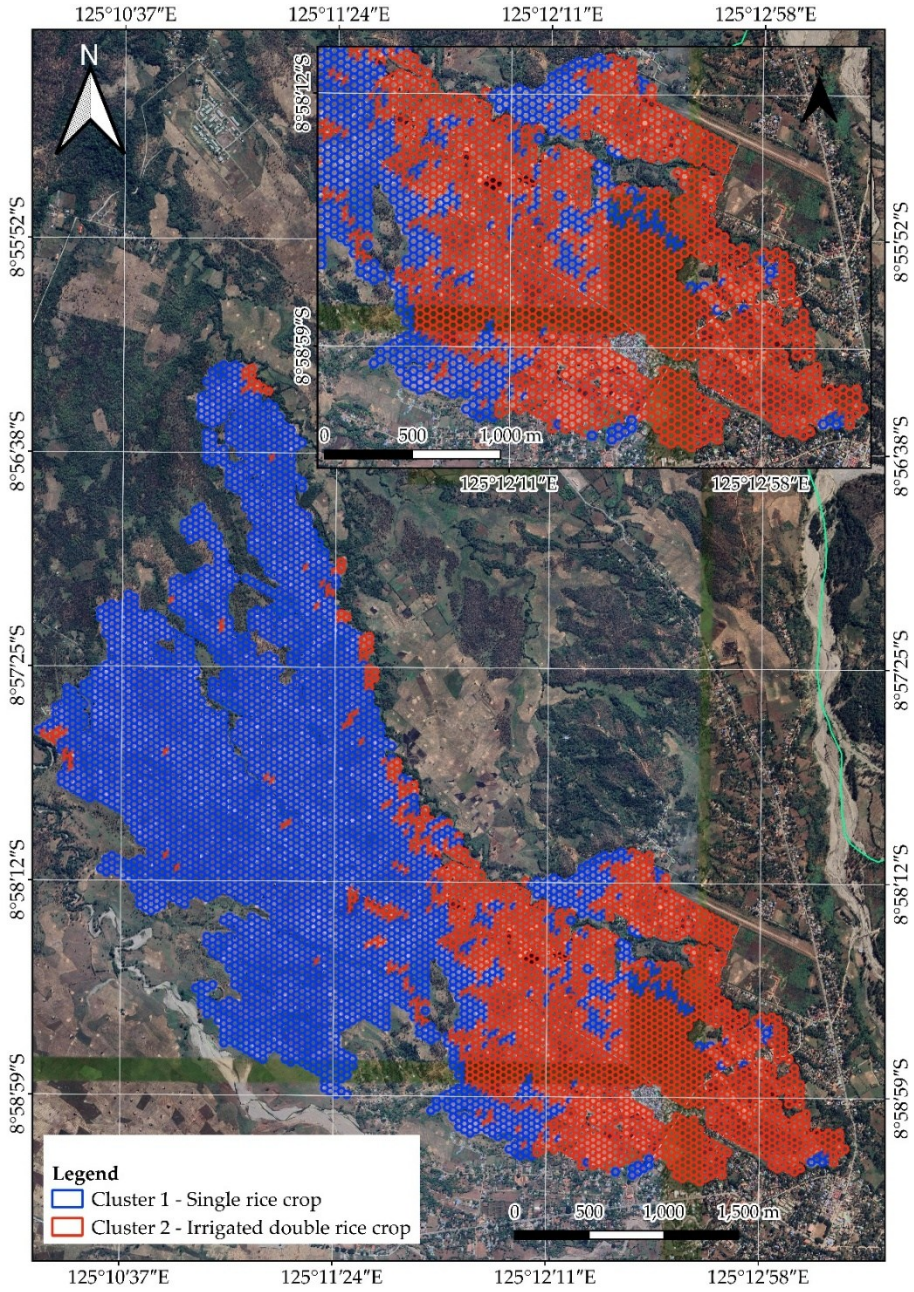


Figure 6: Spatial Distribution Map of Cluster 1 and Cluster 2, represents single rice crop and irrigated double rice crop system, respectively.

**h. Agronomic interpretation and spatial validation of DTW phenology clusters**

Figure 7 provides spatial evidence, with the left panel depicting DTW K=2 cluster assignments across the study area. The right panels display off-season (June to November) PlanetScope NDVI snapshots for 2019 to 2021. Figure 8 offers temporal evidence, presenting monthly NDVI trajectories from December 2018 to September 2022 for Clusters 1 and 2. The main season (December to May) and off-season (June to November) periods are annotated, as well as an NDVI reference line at 0.60.

The figures collectively demonstrate two distinct phenological patterns that correspond to the established cropping calendar in Timor-Leste. The main season extends from December to May, while the off-season spans June to November. During the off-season, Cluster 2 maintains high NDVI values, frequently at or above 0.60 for several months, including August to October in 2019 and 2020, and August to November in 2021, as indicated in Figure 7. This pattern is indicative of a second cropping cycle, consistent with irrigated double cropping systems. In contrast, Cluster 1 remains predominantly below 0.45 during the off-season and does not exceed 0.55, which is characteristic of single-crop areas that are left fallow or exhibit minimal vegetation. The persistent greenness of Cluster 2 in the off-season, as shown in Figure 7, is further reflected in its higher and more stable time-series curve in Figure 8. Cluster 1 displays lower and flatter off-season NDVI values, with the majority of growth occurring during the main season. The consistent observation of elevated off-season NDVI in Cluster 2 and reduced off-season NDVI in Cluster 1 supports the classification of Cluster 2 as 'irrigated double rice crop' and Cluster 1 as 'single rice crop.' Figure 7 identifies the spatial distribution of these systems and their off-season green-up, while Figure 8 details the timing and magnitude of greening from 2018 to 2022. These findings confirm that the DTW clusters are both statistically robust and agriculturally meaningful.

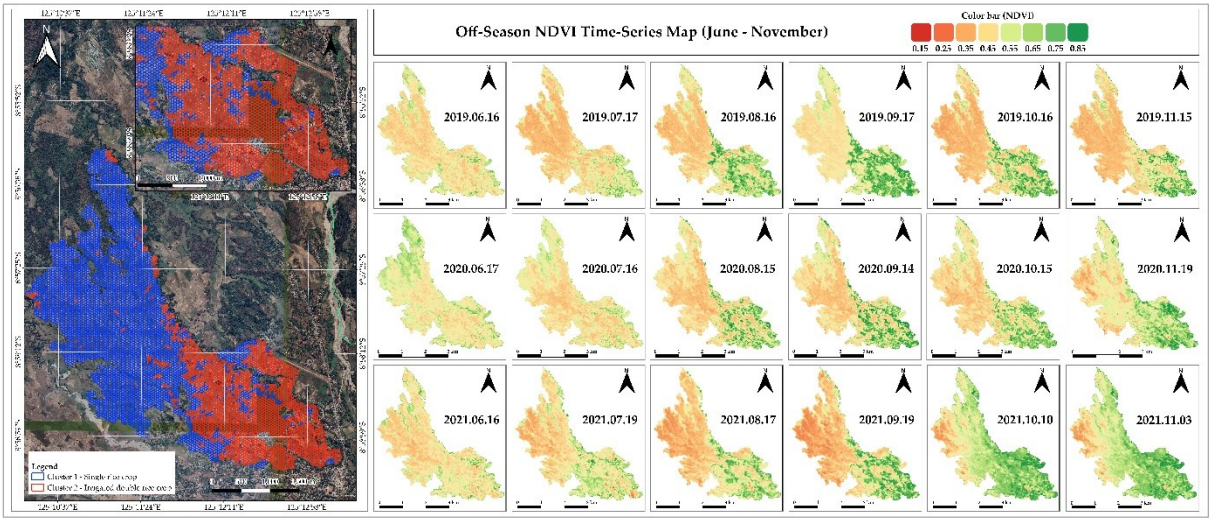


Figure 7: Off-season greenness patterns (NDVI) and DTW-based cluster assignments (K=2) in Maliana, Timor-Leste, 2019–2021.

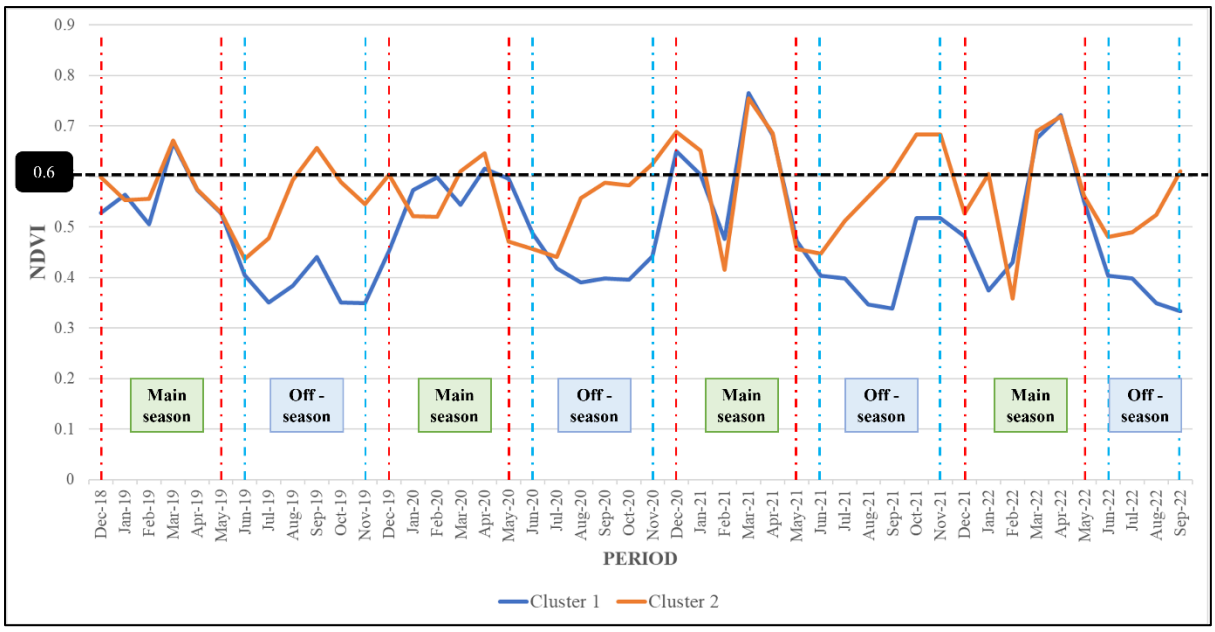


Figure 8: Cluster-level NDVI dynamics (K=2) indicating single- vs. double-cropping seasonality, with main/off-season windows and an NDVI = 0.60 benchmark (2018–2022).

## Conclusion

Monthly PlanetScope (3 m) NDVI data from December 2018 to September 2022, collected across approximately 6,000 hexagonal grid cells, were analyzed using DTW-based clustering to identify coherent phenological structures within the landscape. Multiple internal validation methods, including the Elbow curve, Silhouette scores, and cluster validity indices such as Davies–Bouldin and Calinski–Harabasz, consistently supported a compact and well-separated two-cluster solution (K = 2). These findings demonstrate that DTW-based time-series similarity effectively distinguishes dominant growth dynamics at the field scale in the study area.

Phenology metrics were derived from these clusters, and agronomic labels reflecting seasonal timing and canopy vigor, such as single-versus double-cropping tendencies, were assigned. Visual validation of these labels against high-resolution PlanetScope NDVI revealed spatially coherent patterns and cycle shapes consistent with expected cropping calendars. Collectively, these results support the use of DTW clustering for NDVI time series as a practical, label-light method for indicative mapping of rice phenology in data-scarce environments.

While the workflow is both scalable and transferable, the conclusions remain indicative rather than definitive. The primary limitation is the lack of systematic field observations to calibrate and quantify errors in cluster labeling and phenology metrics. Future research should prioritize

the collection of plot-level ground truth, including sowing and harvest dates, management and irrigation records, GPS photo points, and short transects stratified by cluster, to enhance interpretation and enable robust accuracy assessment.

**References**

Autoridade Munisípiu Bobonaro. (n.d.). Agriculture statistics dashboard. Retrieved August 2, 2025, from https://bobonaro.gov.tl/en/dashboard/

Awong, L. E. E., & Zielinska, T. (2023). Comparative analysis of the clustering quality in self-organizing maps for human posture classification. Sensors, 23(18), 7925. https://doi.org/10.3390/s23187925

Bhatti, M. T., Gilani, H., Ashraf, M., Iqbal, M. S., & Munir, S. (2024). Field validation of NDVI to identify crop phenological signatures. Precision Agriculture, 25, 2245–2270. https://doi.org/10.1007/s11119-024-09998-0

Birch, C. P. D., Oom, S. P., & Beecham, J. A. (2007). Rectangular and hexagonal grids used for observation, experiment and simulation in ecology. Ecological Modelling, 206, 347–359. https://doi.org/10.1016/j.ecolmodel.2007.03.041

Calinski, T., & Harabasz, J. (1974). A dendrite method for cluster analysis. Communications in Statistics, 3, 1–27. https://doi.org/10.1080/03610927408827101

Chen, Z., Wang, W., & Fu, J. (2020). Vegetation response to precipitation anomalies under different climatic and biogeographical conditions in China. Scientific Reports, 10, 830. https://doi.org/10.1038/s41598-020-57663-1

Correia, V. P., & Sarmento, D. R. (2020). Baseline study on the identification of local products in Timor-Leste that have potential for export market and to attract private investments in agriculture sector (pp. 1–18). National Center for Scientific Research (CNIC), UNTL; TradeInvest Timor-Leste.

Davies, D. L., & Bouldin, D. W. (1979). A cluster separation measure. IEEE Transactions on Pattern Analysis and Machine Intelligence, PAMI-1(2), 224–227. https://doi.org/10.1109/TPAMI.1979.4766909

Derrick, T. R., & Thomas, J. M. (2004). Time-series analysis: The cross-correlation function. In N. Stergiou (Ed.), Innovative analyses of human movement (pp. 189–205). Human Kinetics.

Essaadia, A., Abdellah, A., Ahmed, A., Abdelouahed, F., & Kamal, E. (2022). The normalized difference vegetation index (NDVI) of the Zat Valley, Marrakech: Comparison

and dynamics. Heliyon, 8, e12204. https://doi.org/10.1016/j.heliyon.2022.e12204

Fairhurst, T. H., & Dobermann, A. (2002). Rice in the global food supply. Better Crops International, 16(Special Supplement), 3–6

Food and Agriculture Organization of the United Nations. (2011). AQUASTAT country profile—Timor-Leste. https://openknowledge.fao.org/server/api/core/bitstreams/2169f881-507c-4606-9181-30d66ad2941b/content

FAO. 2019. Evaluation of FAO's contribution to the Democratic Republic of Timor-Leste – 2015–2018. Rome.

Food and Agriculture Organization of the United Nations. (2021). Special report—2021 FAO crop and food supply assessment mission (CFSAM) to the Democratic Republic of Timor-Leste (pp. 34–35). https://doi.org/10.4060/cb5245en

Food and Agriculture Organization of the United Nations. (n.d.). Chapter 3 – Rice in human nutrition. Retrieved August 1, 2025, from https://www.fao.org/4/x6905e/x6905e04.htm

Food and Agriculture Organization of the United Nations. (n.d.). GIEWS country brief: Timor-Leste. Retrieved August 2, 2025, from https://www.fao.org/giews/countrybrief/country.jsp?code=TLS.

Fox, J. J. (2003). Drawing from the past to prepare for the future: Responding to the challenges of food security in East Timor. In H. da Costa, C. Piggin, J. Cruz, & J. J. Fox (Eds.), Agriculture: New directions for a new nation—East Timor (Timor-Leste) (pp. 105–114). Australian Centre for International Agricultural Research (ACIAR Proceedings No. 113).

GeeksforGeeks. (n.d.). Elbow method for optimal value of K in KMeans. Retrieved August 1, 2025, from https://www.geeksforgeeks.org/machine-learning/elbow-method-for-optimal-value-of-k-in-kmeans/

Guan, X., Huang, C., Liu, G, Meng, X., & Liu, Q. (2016). Mapping rice cropping systems in Vietnam using an NDVI-based time-series similarity measurement based on DTW distance. Remote Sensing, 8, 19. https://doi.org/10.3390/rs8010019

Hämäläinen, J., Jauhiainen, S., & Kärkkäinen, T. (2017). Comparison of internal clustering validation indices for prototype-based clustering. Algorithms, 10, 105. https://doi.org/10.3390/a10030105

Hossain, M. (2000). The impact of technological change on income distribution in developing countries: A case study on the rice sector in Bangladesh. In R. Barker, R. W. Herdt, & B. Rose (Eds.), The Asian rice economy in transition (pp. 197–216). CABI Publishing. https://doi.org/10.1079/9780851996011.0197

Houborg, R., & McCabe, M. F. (2016). High-resolution NDVI from Planet's constellation of Earth observing nano-satellites: A new data source for precision agriculture. Remote Sensing, 8, 768. https://doi.org/10.3390/rs8090768

Ji, L., & Peters, A. J. (2003). Assessing vegetation response to drought in the Northern Great Plains using vegetation and drought indices. Remote Sensing of Environment, 87, 85–98. https://doi.org/10.1016/S0034-4257(03)00174-3

Kamthonkiat, D., Honda, K., Turral, H., Tripathi, N. K., & Wuwongse, V. (2005). Discrimination of irrigated and rainfed rice in a tropical agricultural system using SPOT VEGETATION NDVI and rainfall data. International Journal of Remote Sensing, 26, 2527–2547. https://doi.org/10.1080/01431160500104335

Kodinariya, T. M., & Makwana, P. R. (2013). Review on determining number of clusters in K-means clustering. International Journal of Advance Research in Computer Science and Management Studies, 1(6), 90–95. Retrieved from https://ijarcsms.com/docs/paper/volume1/issue6/V1I6-0015.pdf

Lampert, T., Lafabregue, B., Dao, T.-B.-H., Smerrette, N., Vrain, C., & Gančarski, P. (2019). Constrained distance-based clustering for satellite image time-series. IEEE Journal of Selected Topics in Applied Earth Observations and Remote Sensing, 12(11), 4606–4621. https://doi.org/10.1109/JSTARS.2019.2950406

Marín Celestino, A. E., Martínez Cruz, D. A., Otazo Sánchez, E. M., Gavi Reyes, F., & Vásquez Soto, D. (2018). Groundwater quality assessment: An improved approach to K-means clustering, principal component analysis and spatial analysis: A case study. Water, 10, 437. https://doi.org/10.3390/w10040437

Mure, S., Grenier, T., Guttmann, C. R. G., & Benoit-Cattin, H. (2016). Unsupervised time-series clustering of distorted and asynchronous temporal patterns. In 2016 IEEE International Conference on Acoustics, Speech and Signal Processing (ICASSP). IEEE. https://doi.org/10.1109/ICASSP.2016.7471879

NASA Earth Observatory. (2000, August 30). Measuring vegetation (NDVI & EVI). NASA. https://earthobservatory.nasa.gov/features/MeasuringVegetation

National Directorate for Agriculture and Horticulture, Ministry of Agriculture and Fisheries, Democratic Republic of Timor-Leste. (2015). Project for agriculture master plan and irrigation development plan: Final report (pp. 120–220). Japan International Cooperation Agency (JICA); Sanyu Consultants Inc.

Reed, B. C., Brown, J. F., VanderZee, D., Loveland, T. R., Merchant, J. W., & Ohlen, D. O. (1994). Measuring phenological variability from satellite imagery. Journal of Vegetation

Science, 5, 703–714. https://doi.org/10.2307/3235884

Rendón, E., Abundez, I., Arizmendi, A., & Quiroz, E. M. (2011). Internal versus external cluster validation indexes. International Journal of Computers, Communications & Control, 5, 27–34.

Rousseeuw, P. J. (1987). Silhouettes: A graphical aid to the interpretation and validation of cluster analysis. Journal of Computational and Applied Mathematics, 20, 53–65. https://doi.org/10.1016/0377-0427(87)90125-7

Rousseeuw, P. J. (1987). Silhouettes: A graphical aid to the interpretation and validation of cluster analysis. Journal of Computational and Applied Mathematics, 20, 53–65. https://doi.org/10.1016/0377-0427(87)90125-7

Runge, J., Petoukhov, V., & Kurths, J. (2014). Quantifying the strength and delay of climatic interactions: The ambiguities of cross correlation and a novel measure based on graphical models. Journal of Climate, 27, 720–739. https://doi.org/10.1175/JCLI-D-13-00159.1

Sasaki, S. (2019). Nutritional characteristics of rice and rice-based diets. Journal of Nutritional Science and Vitaminology, 65(Suppl.), S2–S4. https://doi.org/10.3177/jnsv.65.s2

Seeds of Life Timor-Leste. Agricultural Calendars—Maliana (Bobonaro). Available online: https://seedsoflifetimor.org/climatechange/resources/agricultural-calendars/

Shang, R., Liu, R., Xu, M., Liu, Y., Zuo, L., & Ge, Q. (2017). The relationship between threshold-based and inflexion-based approaches for extraction of land surface phenology. Remote Sensing of Environment, 199, 167–170. https://doi.org/10.1016/j.rse.2017.07.020

Shi, C., Wei, B., Wei, S., Wang, W., Liu, H., & Liu, J. (2021). A quantitative discriminant method of elbow point for the optimal number of clusters in clustering algorithm. EURASIP Journal on Wireless Communications and Networking, 2021, 31. https://doi.org/10.1186/s13638-021-01910-w

Shi, Y., Huang, W., Ye, H., Ruan, C., Xing, N., Geng, Y., Dong, Y., & Peng, D. (2018). Partial least square discriminant analysis based on normalized two-stage vegetation indices for mapping damage from rice diseases using PlanetScope datasets. Sensors, 18(6), 1901. https://doi.org/10.3390/s18061901

Tajunisha, & Saravanan. (2011). An efficient method to improve the clustering performance for high dimensional data by principal component analysis and modified K-means. International Journal of Database Management Systems, 3, 189–197.

Thorndike, R. L. (1953). Who belongs in the family? Psychometrika, 18(4), 267–276. https://doi.org/10.1007/BF02289263

Umaragono, E., Suseno, J. E., & Gunawan, V. G. S. K. (2019, July 24–25). K-means clustering optimization using the elbow method and early centroid determination based on mean and median. In Proceedings of the International Conferences on Information System and Technology (CONRIST) (Vol. 1, pp. 234–240). Yogyakarta, Indonesia.

United States Department of Agriculture, Economic Research Service. (n.d.). Rice sector at a glance. Retrieved August 1, 2025, from https://www.ers.usda.gov/topics/crops/rice/rice-sector-at-a-glance

Wang, X., & Xu, Y. (2019). An improved index for clustering validation based on silhouette index and Calinski–Harabasz index. IOP Conference Series: Materials Science and Engineering, 569, 052024. https://doi.org/10.1088/1757-899X/569/5/052024

World Bank. (2023). Timor-Leste economic report: Charting a new path for growth. World Bank.

Xiao, X., Boles, S., Frolking, S., Salas, W., Moore, B., III, Li, C., et al. (2010). Observation of flooding and rice transplanting of paddy rice fields at the site to landscape scales in China using VEGETATION sensor data. International Journal of Remote Sensing, 31(23), 3009–3022. https://doi.org/10.1080/01431160110107734

Xue, J., & Su, B. (2017). Significant remote sensing vegetation indices: A review of developments and applications. Journal of Sensors, 2017, 1353691. https://doi.org/10.1155/2017/1353691

Zhang, X., Friedl, M. A., & Schaaf, C. B. (2006). Global vegetation phenology from MODIS: Evaluation of global patterns and comparison with in situ measurements. Journal of Geophysical Research: Biogeosciences, 111, G04017. https://doi.org/10.1029/2006JG000217

Zhang, X., Friedl, M. A., Schaaf, C. B., Strahler, A. H., Hodges, J. C. F., Gao, F., Reed, B. C., & Huete, A. (2003). Monitoring vegetation phenology using MODIS. Remote Sensing of Environment, 84, 471–475. https://doi.org/10.1016/S0034-4257(02)00135-9

Zhang, Y., & Hepner, G. F. (2017). The dynamic-time-warping-based k-means++ clustering and its application in phenoregion delineation. International Journal of Remote Sensing, 38, 1720–1736. https://doi.org/10.1080/01431161.2017.1286055